Circulation and Dispersal in California's Borderland Basins

James C. McWilliams[1], Pierre Damien[1], and Faycal Kessouri[1,2]

[1]Department of Atmospheric and Oceanic Sciences, University of California, Los Angeles, CA 90095-1565, USA
[2]Biogeochemistry Department, Southern California Caoastal Water Research Project, Costa Mesa, CA 92626, USA

f

Key Points:

- The borderland basins are semi-isolated, mid-depth depressions in the continental slope.
- They have topostrophic mean currents, variable eddies and tides, and low oxygen concentrations.
- Dissovled materals have a residence time of about one year.

Corresponding author: James C. McWilliams, jcm@atmos.ucla.edu

Abstract

The Borderland Basins off Southern California are semi-isolated sea-floor depressions with connections to each other and to the open Pacific Ocean over narrow sills. A high-resolution, multi-year simulation is analyzed for its currents, stratification, and dissolved oxygen, with a focus on the mean conditions, intrinsic variability, and exchange rates with surrounding waters. The three shallowest, closest basins are given the most attention: Santa Barbara, Santa Monica, and San Pedro. From a combination of multiple means of estimation, the deep basin water mass renewal times are on the order of a year or more, and this time is somewhat shorter in the Santa Barbara Basin than the others.

Plain Language Summary

Off the coast of Southern California are several deep depressions in the continental slope that are somewhat isolated in their currents and chemical water masses, as well as previously having been dumping sites for industrial pollution. The paper presents realistic numerical simulations that show the currents and their variability, as well as the low values of dissolved oxygen distributions and their dynamical influences. The estimated flushing time for their water masses is about a year.

1 Introduction

The so-called Borderland Basins off Southern California are some nine or ten sea-floor depressions at intermediate depths bounded by ridges with narrow sill passages. Some of the ridges emerge as the Channel Islands. The primary question we ask in this paper is how stagnant and isolated are the waters below the sill depths in the three basins closest to the coast: from southeast to northwest, the San Pedro, Santa Monica, and Santa Barbara Basins (hereafter SPB, SMB, and SBB; Fig. 1).

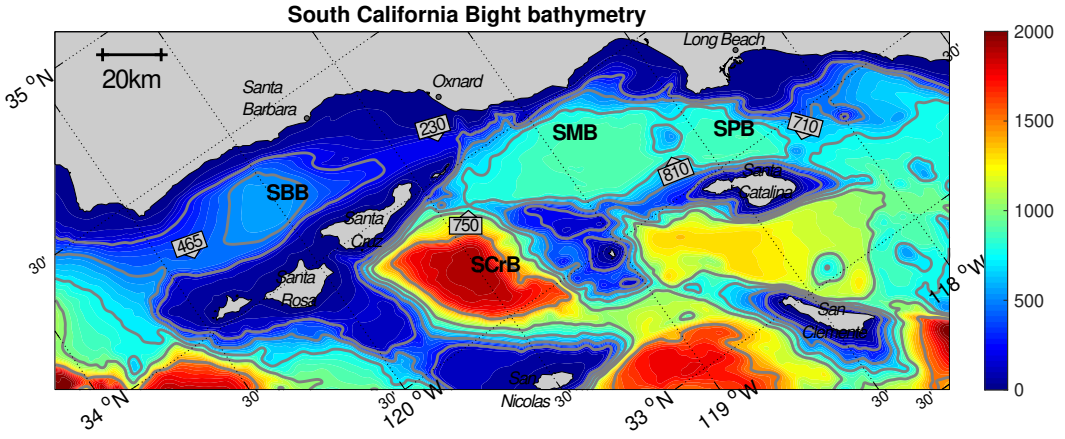

Figure 1. Bathymetry [m] of the Southern California Bight with nearshore basins labeled: San Pedro (SPB), Santa Monica (SMB), Santa Barbara (SBB), and Santa Cruz (SCrB). The major bounding sill depths are in gray boxes, and the gray isobaths have a 250 m interval. The shallower basins' maximum depths are 904 m (SPB), 931 m (SMB), and 590 m (SBB).

A motivation for this question is that the SPB and SMB were sites of Dichlorodiphenyltrichloroethane (DDT) dumping during the 1940s-1960s (Chartrand et al., 1985; Venkatesan et al., 1996), and these deep basins generally contain a heavy human pollution load that accumulates in the sediments (Jackson & et al., 1989; Huh, 1998; Venketesan, 1998;

Schmidt et al., 2024). Another distinction for these basins is that the SMB was the site of a deliberate injection and subsequent tracking of artificial inert chemical tracers in 1985 (Ledwell et al., 1986; Ledwell & Watson, 1991; Ledwell & Hickey, 1995), with the interesting result that the small vertical (*i.e.,* diapycnal, across stably stratified density surfaces) eddy diffusion rate initially measured in the basin interior later became effectively much larger after the tracers had spread laterally and connected with the basin boundary. We also analyze the SBB because of its coastal adjacency and measurement abundance, even though it has not been as heavily polluted by urban waste. All three basins are known to be hypoxic and, at times, anoxic.

The physical oceanography of these deep basins has had limited investigations (*e.g.,* Jackson & et al., 1989; B. Hickey, 1991, 1992; B. M. Hickey, 2000, []). Their waters are weakly stratified and lie well below the pycnocline, and their currents only slightly reflect the patterns of the California Current System and Southern California Eddy that dominate at shallower levels in and above the pycnocline. The most complete description of the currents in the SPB and SMB comes from an abyssal mooring array (B. Hickey, 1991): there is an anticlockwise mean circulation around the edges of the basins; the subtidal eddy variability is an order of magnitude stronger than the mean flow; and the eddies partly reflect coastal-trapped (*i.e.,* topographic) waves with a 10-20 day period. A striking feature of the deep-basin water masses is their episodic rapid "renewal" (*e.g.,* an intrusion of colder, more oxygenated water from offshore) and slow recovery to their more usual water-property values (Emery, 1954; Sholkovitz & Gieskes, 1971; Jackson & et al., 1989; Berelson, 1991; B. Hickey, 1991; Bograd et al., 2002; Goericke et al., 2015; Qin et al., 2022); these events have been seen mostly in temporally sparse hydrographic measurements.

As far as we are aware, no circulation modeling study has been made for these deep basins, although their currents are present but unexamined in many realistic simulations of the California Current System. We choose a high-resolution simulation with a horizontal grid spacing of $dx = 300$ m down-scaled by grid nesting from a multi-decadal hindcast (Kessouri, McWilliams, et al., 2021), as described in Sec. 2. Analysis of this simulation allows further interpretation of previous measurements: the mean circulation (Sec. 3), its variability including the episodic renewal events and low-frequency variability (Sec. 4), and its exchange rates with surrounding waters (Secs. 6-7). Conclusions are summarized in Sec. 8.

2 Model formulation and analysis methods

The oceanic simulations are performed with the Regional Oceanic Modeling System, ROMS (Shchepetkin & McWilliams, 2005) coupled to the Biogeochemical Elemental Cycling model, BEC (Moore et al., 2002). ROMS is a free-surface, terrain-following coordinate model with split-explicit time stepping, based on the Boussinesq and hydrostatic approximations. The subgrid-scale mixing is modeled by the K-Profile Parameterization (Large et al., 1994) and by the numerical diffusion implicit in the upstream-biased advection operator. Two successive configurations are nested in a coast-wide $dx =$ 4 km hindcast simulation (Renault et al., 2021; Deutsch et al., 2021) using offline grid nesting: L1, with a horizontal grid resolution of $dx = 1$ km (Kessouri et al., 2020; Damien et al., 2022, 2023), and L2, with a resolution of of 300 m (Kessouri, McLaughlin, et al., 2021; Kessouri, McWilliams, et al., 2021; Kessouri et al., 2022). The L2 domain spans Southern California, from Tijuana to Pismo Beach, and thus contains the Borderland Basins. It is the primary focus in this paper.

The boundary condition algorithm consists of an active-passive radiation scheme for the baroclinic mode (including T and S) and a modified Flather-type scheme for the barotropic mode (Marchesiello et al., 2001). We use 60 σ levels in the vertical (Shchepetkin & McWilliams, 2009) with grid-stretching parameters $h_{cline} = 250\,\mathrm{m}$, $\theta_b = 3$, and $\theta_s =$

6. Biogeochemical boundary conditions include regional anthropogenic pollution sources (Kessouri, McWilliams, et al., 2021).

Initial and lateral boundary conditions for L2 are derived from the L1 simulation. Hourly surface momentum, heat, and fresh water fluxes are derived from a 6-km Weather Research and Forecast (WRF, Skamarock and Klemp (2008)) atmospheric simulation using bulk formulas modified to include a wind-current coupling parameterization necessary to attain more realistic oceanic mesoscale and submesoscale circulations (Renault et al., 2019). Tidal forcing is prescribed from the TPXO7.1 global tidal prediction model (Egbert et al., 1994) to provide the amplitude and phases for 10 tidal constituents (M2, S2, N2, K2, K1, O1, P1, Mf, and Mm). L2 is run for the time periods from 01/1997-12/2017. The L2 simulation has been validated against a comprehensive database of physical and biogeochemical observations, and provides a realistic representation of physical and biogeochemical cycles in the Southern California Bight in and above the pycnocline and on the continental shelf (Kessouri, McLaughlin, et al., 2021). Here we take advantage of this L2 solution that was devised for other purposes.

The oxygen mass balance (Sec. 6) is diagnosed with monthly time resolution for the period 1997-2012. Its balance equation is

$$\partial_t O_2 \;=\; \underbrace{-\nabla\cdot(\mathbf{u}O_2) \;+\; \partial_z(\kappa_v \partial_z O_2)}_{S_{phys}} + S_{bgc}\,, \tag{1}$$

where the right-side terms are current advection (which includes a small implicit hyperdiffusive effect), explicitly parameterized vertical mixing (with diffusivity κ_v), and the sources and sinks for biogeochemical processes S_{bgc}, including surface air-sea flux, photosynthesis, respiration S_{resp}, and water-sediment flux at the bottom S_{sed}. In the abyss only the latter two processes are significant for S_{bgc}. For brevity we combine the advection and mixing terms in the balance equation into S_{phys}.

Lagrangian trajectories (Sec 7.7.1) are calculated off-line by space-time interpolation in the archived ROMS velocity fields. 100 neutrally buoyant Lagrangian particles are seeded hourly during winter and summer 2000 in the centers of the bottom SMB and SPB. Particles are initially distributed over a region of 2 km diameter. The analysis of this dataset focuses on the vertical escape rate of particles from the deep basin (through an upper level at 700 m depth), and the horizontal escape out of these basins through the vertical extension of the bounding 700 m isobath with extrapolations across the sill gaps. For any given particle, these escapes can only happen once; *i.e.,* re-entries and subsequent new escapes are not counted. The analysis is designed to provide estimates of the deep water dispersal time from a Lagrangian perspective. By mass conservation for the basins, the escape time is also the renewal time. Accurate trajectory positions $\mathbf{X}(t)$ require interpolation between frequently saved Eulerian velocities from the model in the diagnostic integration of

$$\frac{d\mathbf{X}}{dt} \;=\; \mathbf{u}(\mathbf{X},t)\,. \tag{2}$$

A sensitivity analysis shows that a data-saving interval of 1 hour is sufficiently accurate. However, this is storage-intensive (*i.e.,* expensive), and we chose to make these releases only during several months-long periods during the year 2000, which is a period with no major sill overflows (Fig. 14) and thus is indicative of a background rate of escape.

3 Mean stratification, water mass, and circulation

The Southern California Bight has a thin surface boundary layer, shallow pycnocline, and weakly stratified abyss (Fig. 2). The stratification profile is mainly controlled by the temperature. Notice how small the variability is below the sill depths in the deep basins. Measurements at depth are sparse, but there are two long hydrographic time series within the deep basins: San Pedro Ocean Time-series (SPOT; *https://dornsife.usc.edu/spot/data/*)

and California Cooperative Oceanic Fisheries Investigations station Line 81.8 station 46.9 (CalCOFI; McClatchie (2016)). Model-data profile comparisons are in Fig. 3. The deep basin waters are saline, cold, and hypoxic with episodes of anoxia (especially in the SBB). The model profiles are structurally similar to the observed ones, but there are model biases: in nature the salinity stratification is weaker, the temperature is warmer, and the oxygen levels are usually lower. Modeling imprecision at this level of ~ 0.1 PSU in S and 1 C in T is not uncommon, and it is not evident what their particular causes might be here. The O_2 discrepancy level of ~ 10 mmol m^{-3} might be further due to a model underestimation of respiration and sediment-exchange rates in these anomalous local hypoxic environments (Sec. 6); or it might be due to a misrepresentation of the transports by small-scale turbulence and tides. Bottom anoxia can occur in both the SBB and SPB, hence presumably in the SMB as well. The scatter of measurement values suggests that the variability in nature may be somewhat larger than in the model, but sampling and instrument errors cannot be ruled out. A comparison with time series measurements for SPOT (Fig. 3) show that the top-to-bottom O_2 difference and surface seasonal cycle are about right and that at least some of the surface measured O_2 values seem anomalous. (The O_2 trends over this period are quite weak.) These model biases do not seem excessive, and we will proceed to analyze the simulation as if it is mostly reliable in its processes and phenomena within an acceptable level of imprecision.

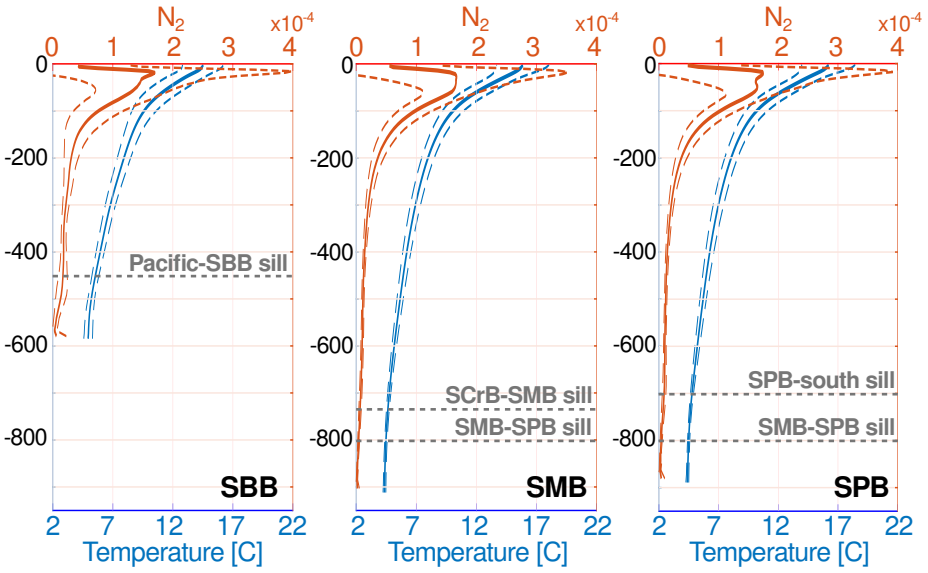

Figure 2. Depth [m] profiles of simulated temperature (blue) [C] and stratification N^2 (red) [s^{-2}], from left to right, in the middle of the SBB, SMB, and SPB. Solid lines are mean profiles averaged over 15 years from 1997 to 2012, and dashed lines are the incremental daily-mean RMS (root-mean-square variability). The profiles terminate at the basin bottoms, and bounding sill depths are marked.

The simulated water-mass property relations are in Fig. 5. The $T-S$ curves are remarkably linear, with slightly fresher and colder water to the north and seaward. The $T-O_2$ relations are also rather linear but only above the basin sill depths; below they curve toward warmer, less oxygenated water, compared to farther seaward, indicating a degree of transport isolation for these bottom waters. The SBB has a $T-S$ curve very close to that of the adjacent Pacific, suggesting a rather weak transport barrier between them. The SMB and SPB are warmer and saltier than the Pacific, as well as remark-

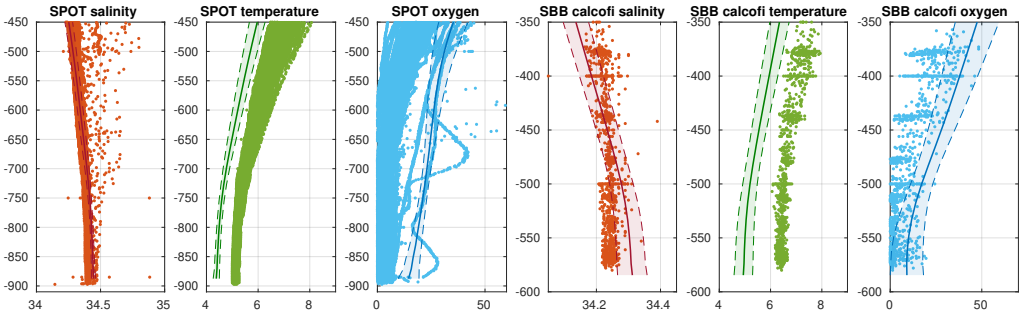

Figure 3. Depth [m] profiles in the basin centers for mean salinity $S(z)$ [PSU], temperature $T(z)$ [C], and oxygen $O_2(z)$ [mmol m^{-3}], compared to measurements in the SPB (SPOT) and SBB (CalCOFI). The measurements are depicted as dots, and the model's mean and standard deviation are solid and dashed lines with light shading in between.

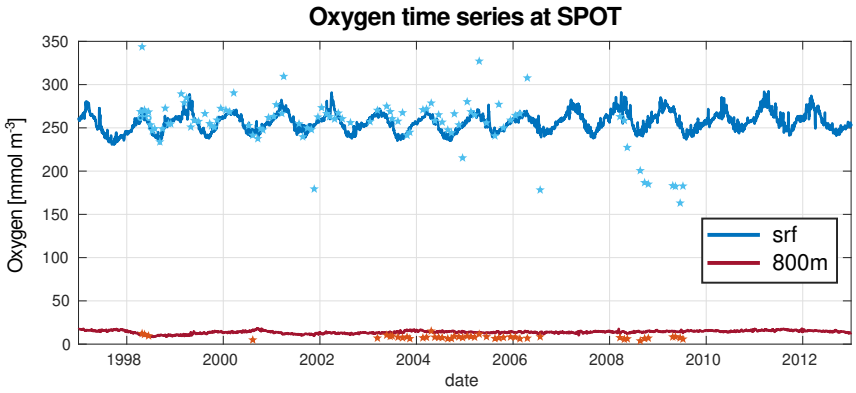

Figure 4. Oxygen time series at (blue) the surface and (red) 800 m at the SPOT location (SPB), compared with SPOT measurements depicted by stars.

ably similar to each other; this shows an efficient exchange between them, consistent with the very low sills separating them (Fig. 1). While the SBB has only a marginally smaller mean bottom O_2 compared to the SMB and SPB, it occurs at a shallower depth and warmer T, which we interpret as due to its higher local export production and greater respiration rate (Sec. 6). All of these Borderland Basins are depleted in O_2 compared to the Pacific, even up to the bottom of the pycnocline at around $T = 8$C (Fig. 2), well above the bounding sills. The oxygen curvature below the sills is indicative of water-mass isolation, where the dissolved oxygen content is respired while renewal processes are limited. Comparing the oxygen levels above the sea floor in the different basins shows evidence of larger respiration rates or lower ventilation process (Sec. 6).

As noted by B. Hickey (1991) for the SMB, the mean horizontal circulations are anticlockwise (*i.e.,* prograde in the sense of Kelvin or topographic Rossby wave propagation) in all three deep basins (Fig. 6). They are generally on the order of a few cm s^{-1}, strongest on the basin edge slope and going over the bounding sills, and nearly zero in the basin interior. In the SBB and SPB the edge slope current comes close to completing a circuit around the basins, but in the SMB the circuit is clearly broken on the shoreward side. The simplest interpretation of this is as eddy-driven mean currents, as in the "Neptune" model based on statistical mechanical equilibria and potential vorticity mixing (*e.g.,* Merryfield et al., 2001). The occurrence of prograde mean currents on

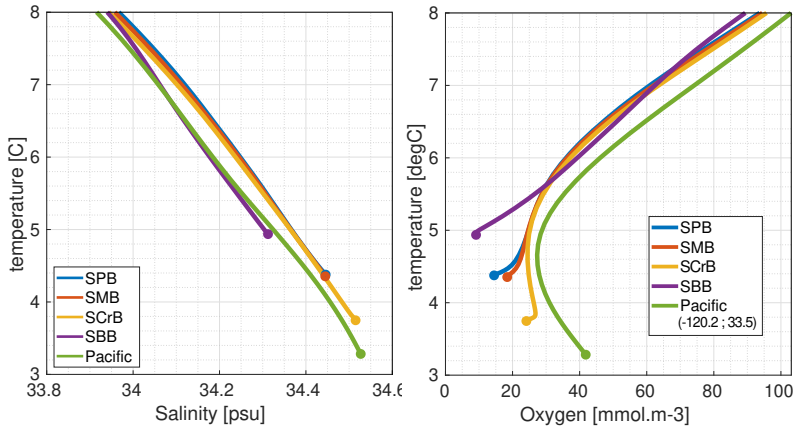

Figure 5. Mean profiles of temperature *vs.* salinity (left) and temperature *vs.* oxygen (right) in the centers of the Borderland Basins compared to farther offshore (Pacific profile).

abyssal slopes is widespread in realistic simulation models; it is now more generally referred to as topostrophy (Capó et al., 2024; Schubert et al., 2024).

The mean current speed decays upward from the bottom on a scale $\sim$ 100 m. These flow patterns are dissimilar to the generally northwestward path of the California Undercurrent that occurs at shallower depths. The mean vertical velocities are similarly largest on the edge slopes (Fig. 6). However, they are quite weak, $\sim 10^{-4}$ m s^{-1}, and alternate in sign; their horizontal-area means are quite weak and vary with depth.

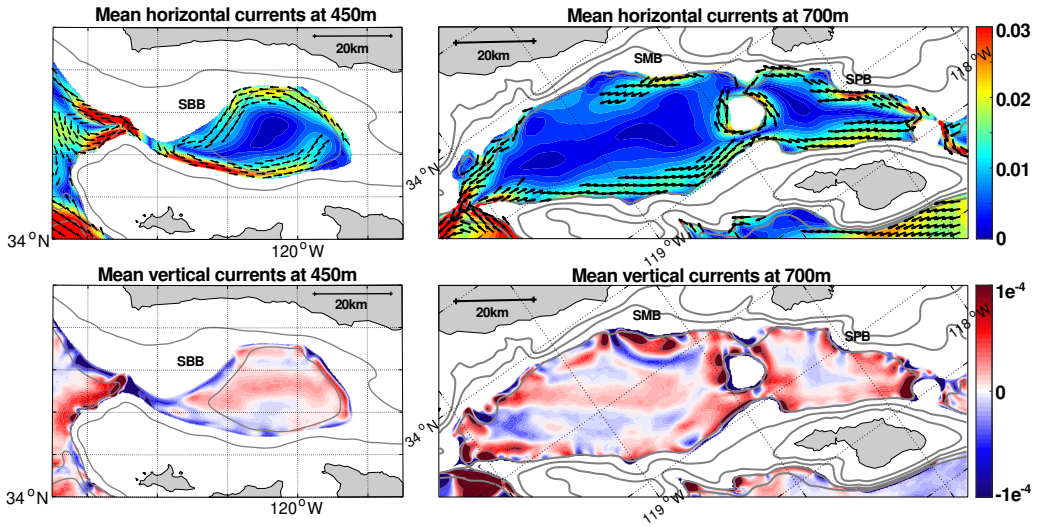

Figure 6. Near-bottom mean currents: horizontal (top) and vertical (bottom); the SBB at at z = - 450 m (left) and the SMB+SPB at z = - 700 m (right). The horizontal velocity has speed in color and direction in arrows for speeds above 0.01 m s^{-1}.

The basin-bounding sills are sites of relatively strong mean currents, both horizontally and vertically. The mean cross-sill currents (Fig. 7) in all cases have inflow on the south and west sides of the sill passage and outflows on the north and east sides. They can be as strong as 0.03 m s^{-1} near the bottom. They are only a few km in width. These are geostrophic flows that lean against the slope on their rightward side (northern hemisphere), as is similar for estuary passage flows, and is a further manifestation of topostrophy. The cross-passage integrated through-flow transport is relatively weak and also varies with height above the sill minimum elevation. In particular, there is a hill in the middle of the sill between the SMB and SPB, around which there is a clockwise circulation, again consistent with Neptune. Thus, there are available mean pathways over the sills, both in and out (and between for the SMB-SPB) of the separate basins.

This is an exchange process that acts to limit the water-mass isolation within the basins. If the individual sill currents are viewed as drainage currents (rather than recirculations), then they could renew the volume of bottom water within a period on the order of a year.

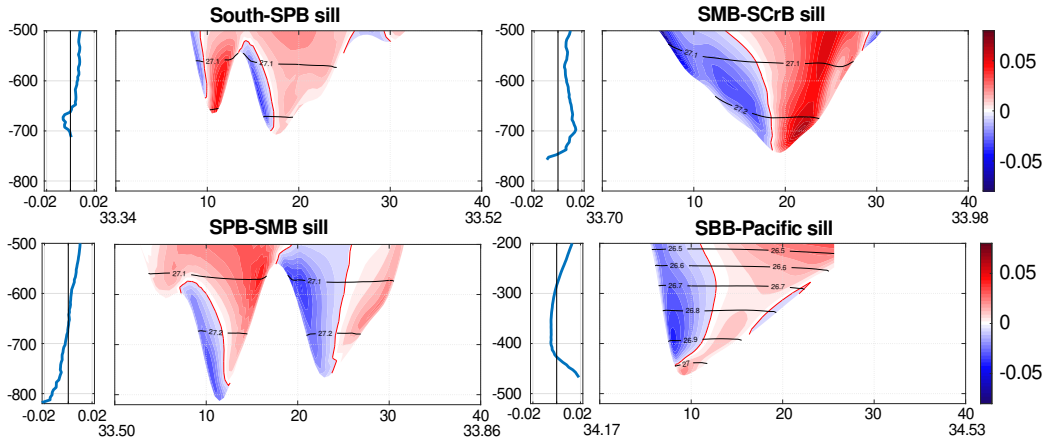

Figure 7. Mean velocity cross-sections [m s^{-1}] at the major sills for the three basins. Currents are defined positive westward or northward for the component perpendicular to the sill section. The line plots to the left of each section 'are vertical profiles of the horizontal average velocity across the plotted section at that depth. The thin black lines are adiabatic isopycnals, labeled in σ_0 units [kg m^{-3}, *i.e.,* the density anomaly of sea water at atmospheric pressure].

Few velocity measurements have been made in the deep basins. In the SMB and SPB, the mean current intensity decreases rapidly below 250 m depth. Jackson and et al. (1989) and B. Hickey (1991) report a anticlockwise circulation with magnitudes ranging from 0.005 to 0.01 m s^{-1} at about 700 m. This is slightly lower than the ROMS mean velocities, estimated in a 5 km wide edge band at 0.011 m s^{-1} (+/- 0.006). Over the sills, the measured average currents are larger: $\sim$ 0.065 m s^{-1} over the SCrB-SMP sill, $\sim$ 0.022 m s^{-1} over the SMB-SPB sill (0.022 m s^{-1} in Jackson and et al. (1989)), and $\sim$ 0.016 m s^{-1} over the South-SPB sill.

4 Variability

There is a substantial variability in the currents, ranging from tides to interannual variability, and punctuated by sill overflow events.

The spatial pattern of current fluctuations at depth (Figs. 8-9) is similar to the mean currents in the sense that speeds are larger around the basin edges and near the sills than in the centers. The amplitudes are somewhat larger than the mean, reaching 0.1 and 0.4 $\times 10^{-3}$ m s^{-1} in a few places for horizontal and vertical velocities, respectively. With a partition into daily-average (eddy) and supra-daily (mostly tidal) components, the velocity amplitudes are similar, except that the tidal currents in the SBB are rather weak (especially in w). Compared to eddy horizontal currents at a similar depth outside the basins (*e.g.,* west of the SBB), the within-basin currents are weaker. The vertical velocities are even more spatially heterogeneous and concentrated near the basin edges than are the horizontal ones.

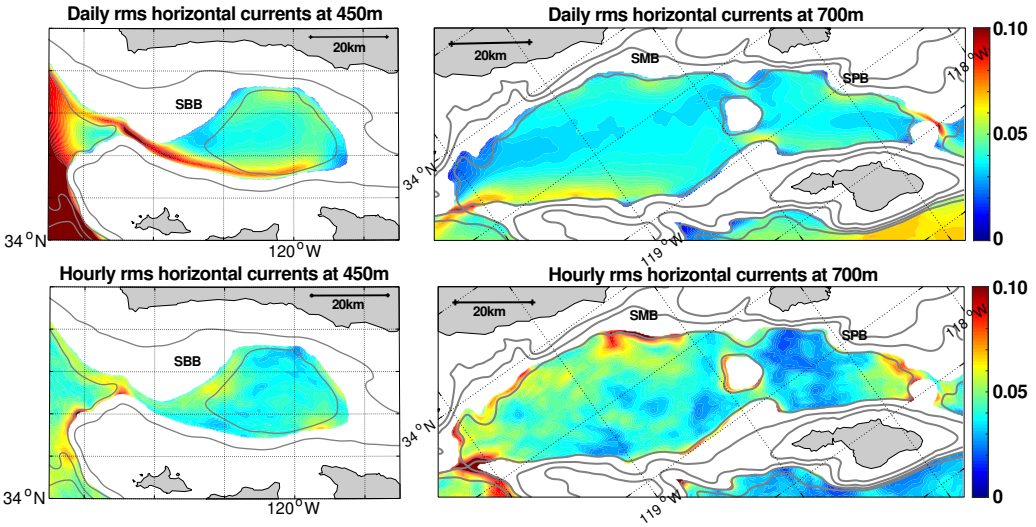

Figure 8. RMS horizontal velocity variability [m s^{-1}] for daily-averaged currents minus the time-mean over a 15-year interval (top row) and for the hourly residual during January 2000 (mostly tidal; bottom row) in the SBB at 450 m (left column) and in the SMB+SPB at 700 m (right column).

B. Hickey (1991) associates the subtidal fluctuations on the edges of the SMB and SPB with coastal trapped waves (CTWs) propagating counter-clockwise with peak velocities of about 0.04 m s^{-1}. The identified CTW time scale is between 10 and 20 days with a phase propagation speed between 0.1 and 0.4 m s^{-1}. CTWs are linear topographic Rossby wave eigenmodes that propagate along a slope in a prograde direction (A. Robinson, 1964; Allen, 1975; Mysak, 1985). In the numerical simulatoin, a visual impression of a subtidal velocity field is of messy patterns, but a cross-spectral analysis, as described in Fig. 10, confirms the existence of CTWs as a modest fraction of the eddy variability.

The vertical scale of the abyssal eddies and tides is rather large, $\geq$ 100 m (not shown). However, the correlations with surface and pycnocline subtidal currents is not high, along with being much weaker by nearly an order of magnitude (Fig. 11). Our sense is that these deep eddy currents are mostly due to the general mesoscale variability in the Bight, with local modifications by interaction with the topographic shape. Together these features seem consistent with the idea of an eddy-driven mean flow (Sec. 3).

At the sills (Fig. 12), the eddy $v(t)$ and $T(t)$ time series have a broad frequency spectrum. v fluctuations are $\sim$ 0.1 m s^{-1}, and T fluctuations are $\sim$ 0.3 C. Daily-mean

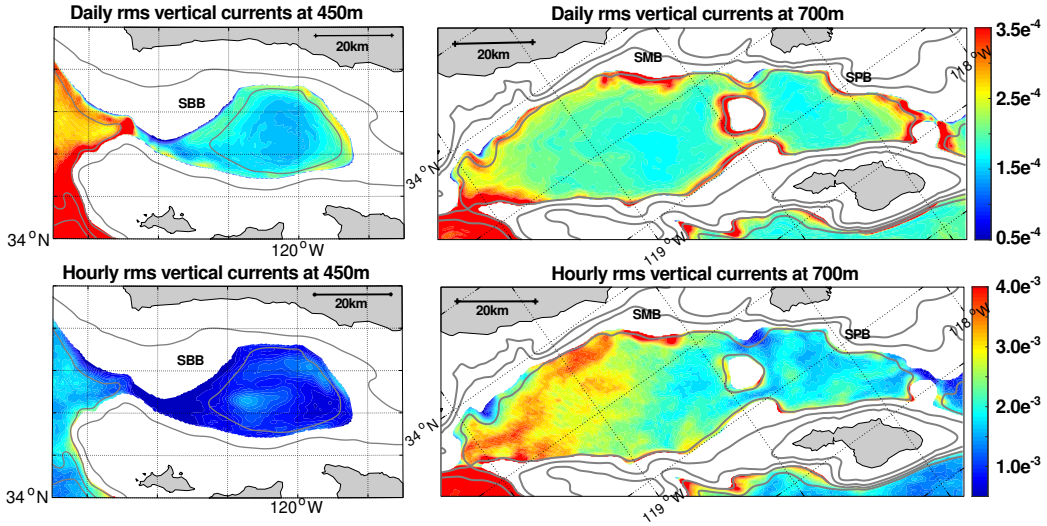

Figure 9. Same as Fig. 8 except for vertical velocity.

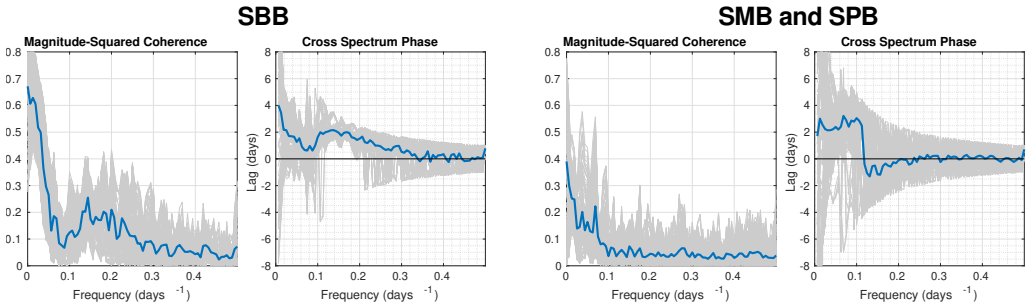

Figure 10. Evidence of coastal trapped waves (CTWs): (gray lines) multiple cross-spectral analysis for along-isobath deep current time series located around the basin on the same isobath and equidistant from one another: 210 pairs of time series are analyzed around the SMB and SPB with a spacing of 63 km; and 110 pairs are analyzed around the SBB with a spacing of 33 km. The blue line shows the average signal of the multiple cross-spectral analysis. The blue line shows the average signal of the multiple cross-spectral analysis. The magnitude square coherence shows a significant coherence in the spectral analysis for frequencies lower than 0.1 day^{-1}. In the SBB, it is associated with a time lag of 2-5 days, which corresponds to a phase velocity of 0.08-0.2 m s^{-1} in the prograde direction, consistent with CTWs. This is higher than the signal of an advected eddy, because the mean flow is about 0.01-0.02 m s^{-1} at 450 m. In the SMB and SPB, the time lag is remarkably constant for frequencies lower than 0.1 day^{-1}: between 2 and 4 days. It corresponds to a phase velocity of 0.15-0.30 m s^{-1}, again much larger than the mean flow.

and monthly-mean amplitudes are similar. The fluctuations are largest at the SBB-Pacific sill, probably due to the large eddy variability in the offshore Pacific waters (Fig. 8, upper left), and they are lowest at the interior SMB-SPB sill, which is the most isolated passage within these three deep basins. The tidal $v(t)$ signal is much stronger than its $T(t)$ counterpart (not shown). These sill v fluctuations do provide pathways for "eddy-diffusive" exchanges between the deep basins and surrounding waters. There is little evidence of a seasonal cycle. The interannual variability is not very strong, although the

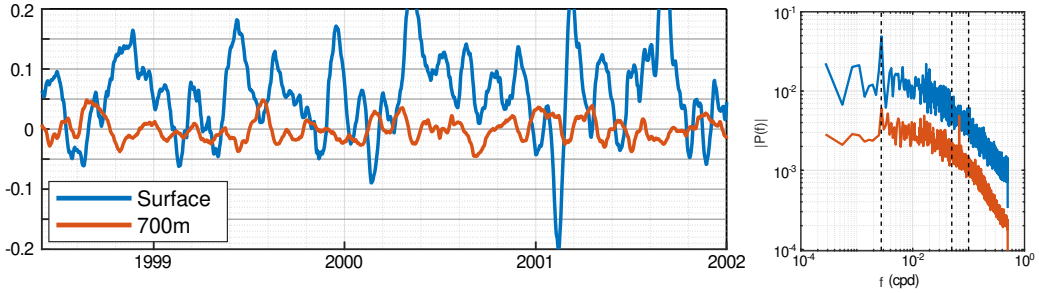

Figure 11. (Left) time series of along-isobath velocity $[ms^{-1}]$ at the surface and at 700 m depth on the northeast slope in the SMB with a 10 day low-pass filter and (right) their frequency spectra for daily-averaged values averaged over multiple sites along the same isobath in the SMB and SPB. The dashed vertical lines are periods of 1 year, 20 days, and 10 days. The correlation between these time series is insignificant.

1997-98 El Niño - Southern Oscillation (ENSO) event is evident in all the T series, and perhaps even more weakly in v. Also, T is warmer over multiple years during the period of 2002-2008.

As a further exploration of low-frequency variability, the seasonally-averaged RMS horizontal velocity in the basins is tracked over the 15 year period (Fig. 13). From year-to-year the level of eddy variability can be quite different, but there is no evidence of a mean seasonal cycle at the bottom of the deep basins.

The principal observational evidence for deep basin currents is in Jackson and et al. (1989) and B. Hickey (1991). Seen in the context of Figs. 12-13, they are certainly under-sampled. Nevertheless, we see a general quantitative consistency between these measurements and our simulated currents.

5 Flushing events

As mentioned in Sec. 1, several instances of large changes in the deep water-mass properties have been detected in the Borderland Basins, referred to as flushing events. They occur in the simulation as well (Fig. 14). In all three basins, events of a sudden drop in $T \sim$ 0.1-0.5 C and increase in $O_2 \sim$ 10-30 mmol m^{-3} occur irregularly at intervals between a fraction of a year to multiple years. In a flush the water comes from the adjacent Pacific waters that are colder and more oxygenated (Fig. 5); it flows over the basin sills and penetrates into the basin interior, with fairly rapid lateral spreading by eddy stirring. The flushes are stronger and more frequent in the SBB compared to the SMB and SPB, indicating a greater degree of penetration of currents from offshore over its rather low western sill.

The 1997-98 ENSO event has simultaneous flushes in all three basins, indicating its widespread impact along the coast. Most of the other flushes occur at least partly independently among the basins, indicating more local advective anomalies. Apart from the ENSO event, the property changes are largest in the SBB, intermediate in the SMB, and smallest in the SPB. This variance is an additional indication of varying degrees of direct connectivity with the open Pacific Ocean.

An important issue is the residence time of water in the deep basins, in particular its dispersal into the wider ocean (Sec. 7), *e.g.,* for dissolved pollutants. The flushing events in Fig. 14 exhibit an abrupt onset (days-weeks) and a slow relaxation back

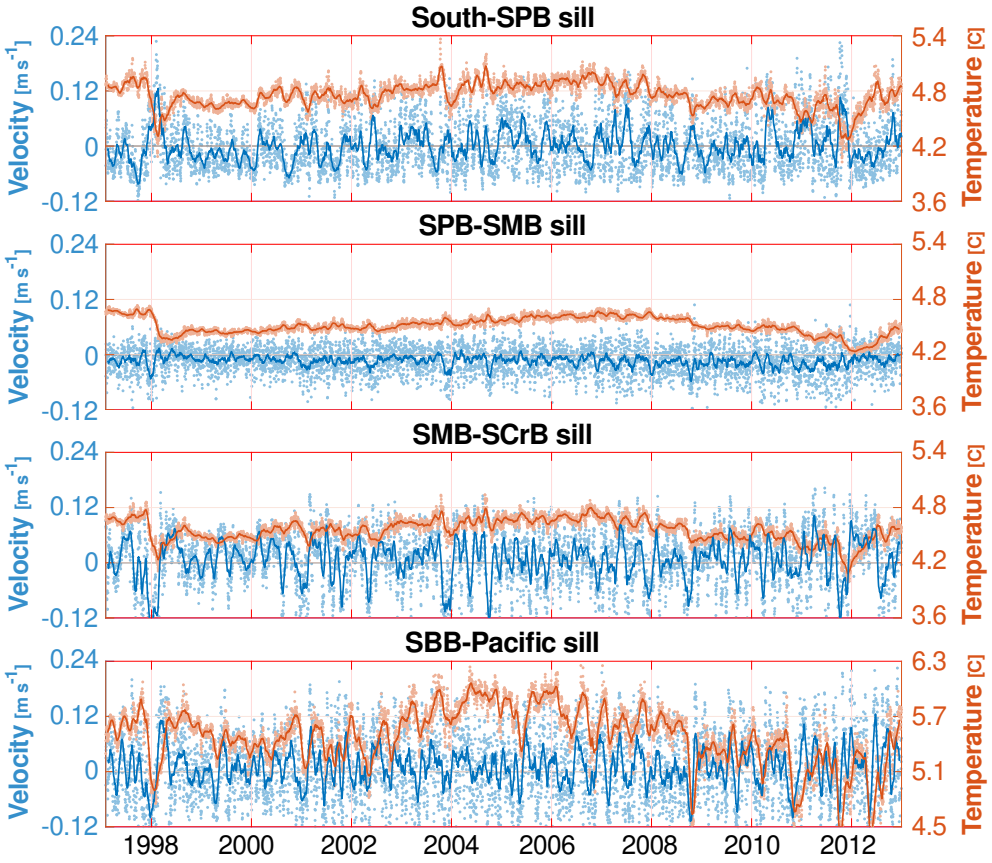

Figure 12. Time series of (blue) deep current and (red) temperature at the major sills for the three deep basins. Currents are defined positive westward or northward for the component perpendicular to the sill section. Time series are computed by averaging the velocities and temperatures across the sections over the first 30 m above the sill floor to represent exchanges between basins across the sills. Dots are daily-mean values, and solid lines are monthly-mean values with a 31-day moving window.

to more equilibrium conditions (months-years). The latter is indicative of the primary dispersal escape time (Sec. 7), although some material can escape more quickly if connected to the sill exchange flows (Figs. 7 and 12).

The flushes are overflow currents driven directly by a horizontal pressure difference across this sills, which in turn is most likely associated with passing mesoscale eddies (Fig. 15). The eddies themselves are mostly in geostrophic balance above the sills, but the sill geometry interrupts this balance for the currents near the bottom while the pressure signal extends to the bottom and provides an unbalanced force. This phenomenon is similar to that of pressure-driven flows across mountain gaps, *e.g.,* the Santa Ana wind in Southern California (Hughes & Hall, 2010). Notice that this relation holds equally for sill transports of both signs, both inward (flush) and outward flows. In contrast, the flushes during the large ENSO event in 1997-8 (Fig. 14) is a larger-scale event spanning all three basins. The time series of temperatures above the sill and in the basin center indicate a typical time lag of a week or so in most instances of a sill inflow event. This indicates an efficient process of horizontal stirring and mixing within the basins, usually starting with a pulse in the anticyclonic edge current, then spreading into the interior; illustrations are in the movies included in the Supplemental Information.

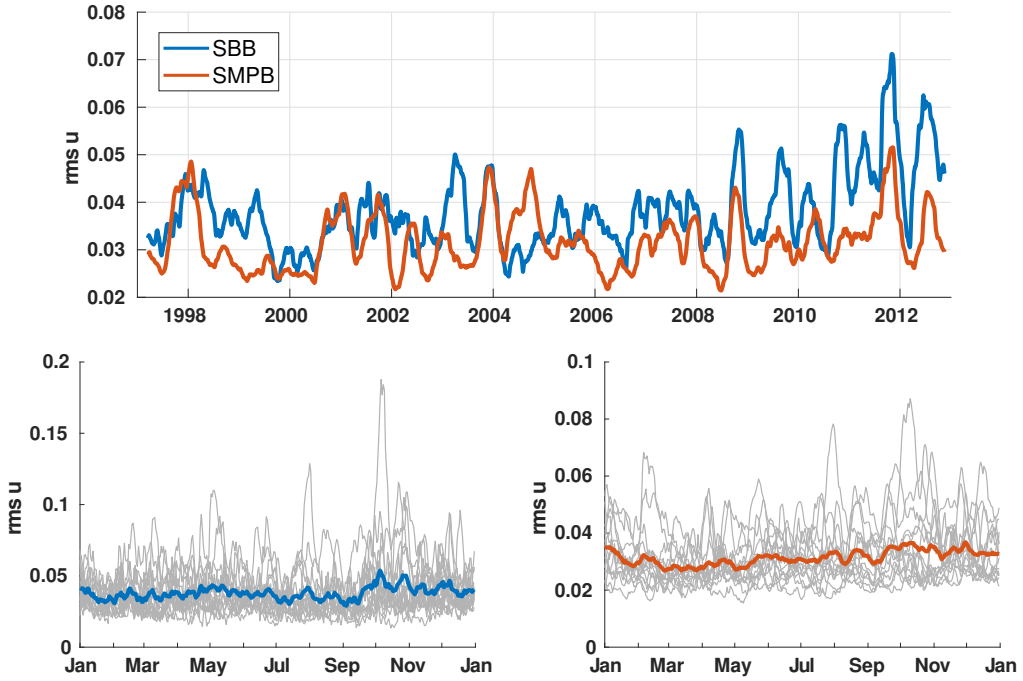

Figure 13. (Upper panel) Time series of the spatially-averaged RMS deep horizontal velocity in the (blue) SBB and (red) SMB+SPB. The signal is computed with a 3-months moving window to emphasize low-frequency variability. (Lower panels) Seasonal cycles of the spatial RMS of deep currents in the two basins (SBB on left; SMB+SPB on the right), both averaged (blue and red lines) and for the individual 15 years (gray lines).

6 Oxygen balance

Physical transport rates also can be determined from their effect on material concentrations. Although the model has an extensive set of biogeochemical cycles (Deutsch et al., 2021), here we analyze only the dissolved O_2 balance, partly because it has more measurements than other material concentrations and partly because it is distinctive in the deep basins for its low values (Figs. 14 and 5). In addition, subtle changes in the oxygen level of these deep and isolated basins have a fundamental influence on the benthic biota dynamics and sediment fluxes of essential micro-nutrients, as iron (D. Robinson et al., 2024) and sulfur (Yousavich et al., 2024), modulating the deep chemical cycling. Oxygen is also a valuable tracer for estimating residence time in the deep ocean. When a water parcel is subducted below the surface layer, then no longer exposed to photosynthesis and isolated from the atmosphere, its oxygen content decreases. The consumption rate depends on both the bacterial activity responsible for respiration and on the burial in the sediments.

In the Southern California Bight oxygen depletion rates are high. The combined effects of seasonal and synoptic upwelling, lateral advection within the California Current System, anthropogenic influences, and orographic winds shaped by the presence of islands collectively contribute to a significant nutrient supply in the euphotic zone. This nutrient enrichment fuels elevated rates of primary production. The generated organic matter settling leads to high sedimentation rates (Collins et al., 2011; Kemnitz et al., 2020), and its subsequent degradation, both in the water column and sediments, causes considerable oxygen depletion in the abyssal waters (Chavez & Messié, 2009). As a re-

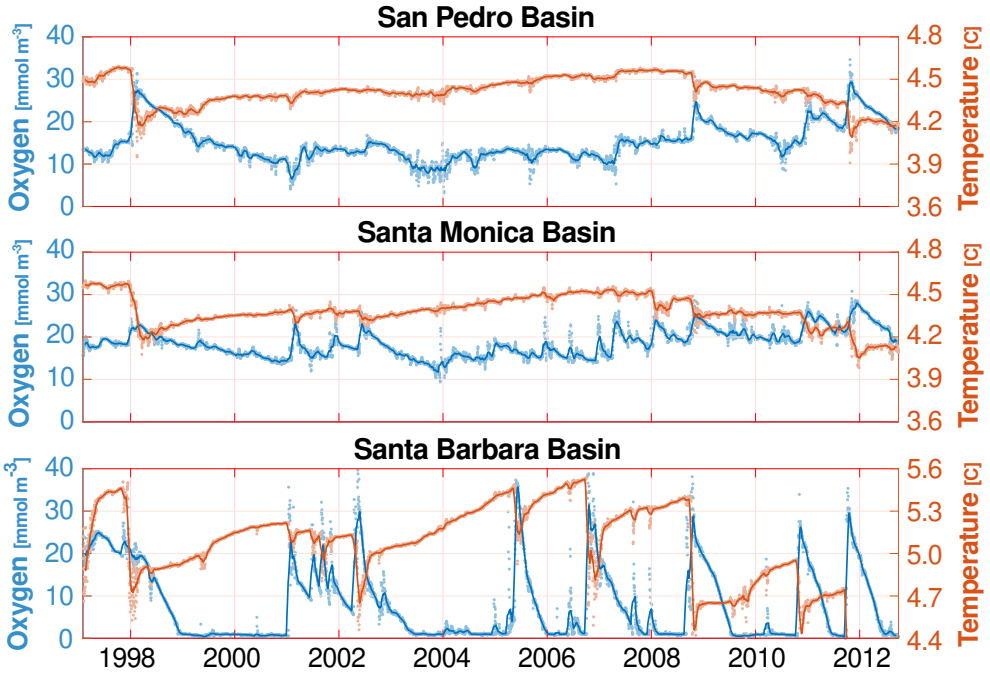

Figure 14. Time series of oxygen [mmol m^{-3} (blue) and temperature [C] (red) in basin centers at the bottom. Dots are daily-mean values, and solid lines are monthly-mean values with a 31-day moving window. The flush magnitudes in concentration are larger in the SBB and than in the SMB and SPB.

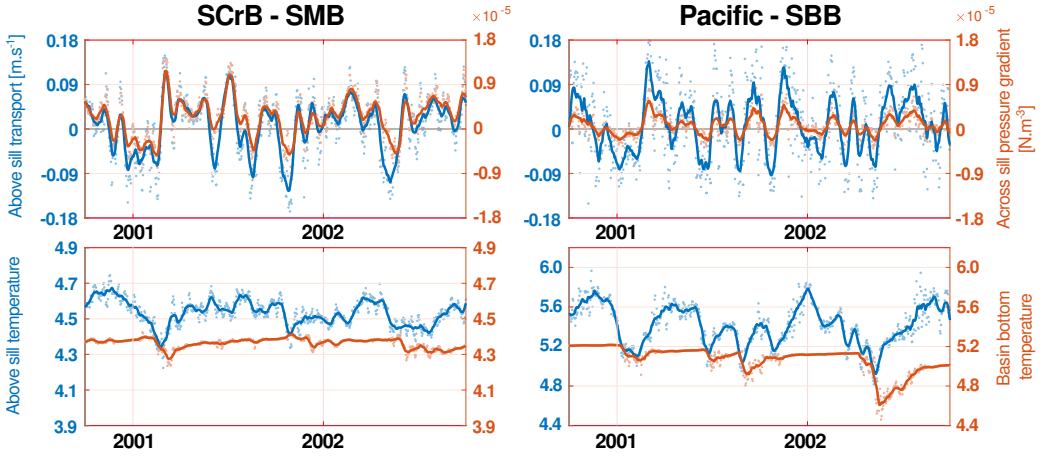

Figure 15. (Upper panels) Relation between above-sill transport (negative inward) and the pressure gradient across the sill over a horizontal distance of 7 km for the ScrB-SMB sill and 10 km for the Pacific-SBB sill. On each side of the sill, the pressure is averaged over a 3 km radius area in order to smooth small scale fluctuations and evaluate the larger scale cross-sill gradient. (Lower panels) Temperatures above the sill and at the bottom center of the basin. The time series are shown at the SCrB-SMB and Pacific-SBB sills for a 2-year period.

sult, these deep basins experience regular low-oxygen conditions (White et al., 2019; Valentine et al., 2016; Hamersley et al., 2011).

In the Eulerian reference frame of the numerical simulation, the oxygen balance (1) involves the physical transport S_{phys} that includes the advection by currents and mixing processes, and the biogeochemical sources and sinks which in the deep basin are the respiration in the water column S_{resp}) and in the sediment flux S_{sed}. In Fig. 16 a balance analysis is made with a monthly time step and in a volume integral for the combined SMB and SPB for the water below z = - 700 m depth and bounded by the 700 m isobath with transects across the sills; an analogous analysis is made for the SBB using the z = - 450 m. The right-side terms are plotted as point-wise rates [$mmol\, m^{-3}\, s^{-1}$]. S_{phys} is a source transporting higher oxygen water into the deep basin, and S_{sed} and S_{resp} are sinks. The physical transport source, dominated by the advection, exhibits the greatest time variability. S_{sed} is much larger than S_{resp}, and their smaller degree of variability has an evident seasonal cycle associated with the upwelling and surface-layer productivity cycle. In a time average, these three terms sum to nearly zero, and their monthly imbalances imply the rate of concentration change on this time scale, dO_2/dt. Intra-seasonal S_{phy} fluctuations are large and imprint on the O_2 temporal variations. A distinctive feature is a large monthly S_{phy} peak generating a sudden overall oxygen ventilation, evidenced by a dO_2/dt positive peak; however, the background modes of S_{phys} variability are less clear and may simply be mesoscale eddy transport variability. These events correlate well with the large over-sill flows responsible for the deep water renewal, and thus deep oxygen ventilation. This correlation is particularly clear in the SMB and SPB, where the rate magnitude and variability are lower than in the SBB. The local rates in the SBB are much higher than the SMB+SPB, reflecting its greater exposure to exchange with Pacific waters, its shallower depth, and its greater export production (Kessouri et al., 2022). As a results of its larger oxygen depletion rate, the SBB is thus particularly exposed to hypoxia, and its anoxic events are more frequent (Fig. 14).

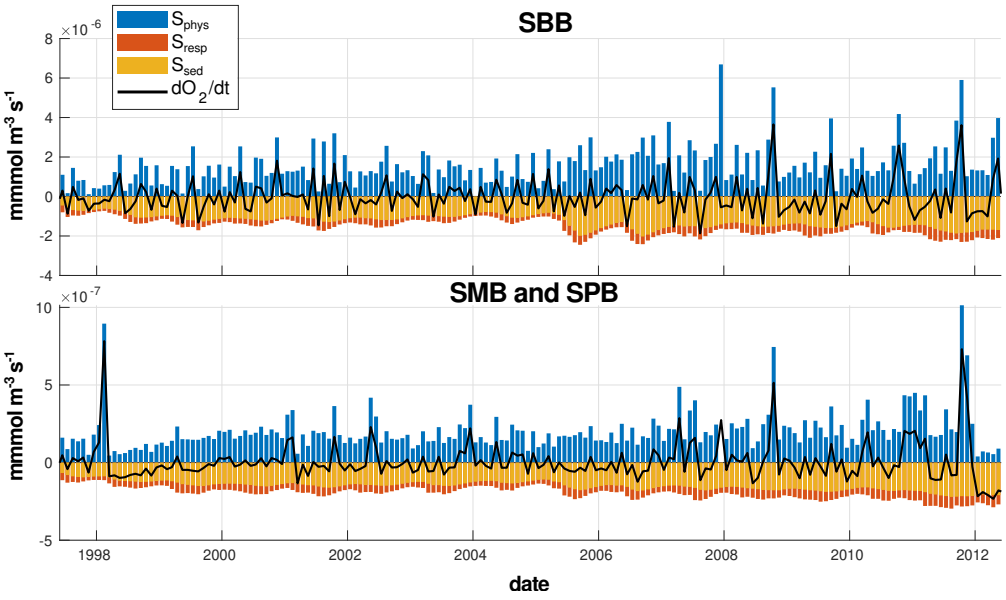

Figure 16. Time series of volume-averaged source terms [mmol m^{-3} s^{-1}] for the O_2 balance in the SBB (top) and the SMB+SPB (bottom). The positive dO_2/dt (black line) is associated with increased O_2 transport that partly correlates with sill overflows.

As mentioned in Sec. 3, the simulation has a modest bias of excess O_2 values at the bottom of the basins, which implies that its O_2-balance estimates should be viewed with some skepticism. Both S_{resp} and S_{sed} are uncertain and there is little specific in-

formation about these in the deep basins. Observational estimates of sediment oxygen utilization are scarce and rather uncertain due the technical difficulties of measuring in such oxygen-depleted conditions. Also, the observations in different sub-basins of the Bight indicate considerable variability due to difference in ambient seawater oxygen and accumulation of organic matter. In the model, S_{sed} uses a very simple oxygen sediment exchange rate linearly proportional to the modeled organic carbon concentration in the sediment (Deutsch et al., 2021). In the SMB, it provides fluxes in reasonable agreement with the measurements reported in (Jahnke, 1990) ($\approx 0.5 \times 10^{-5}$ mmol m^{-2} s^{-1}; see the supplementary Table S1 in Jørgensen et al. (2022)). However, it seems reasonable to think that they might be low, also recognizing that a large uncertainty is usually associated with measured respiration rate estimates (Craven & Jahnke, 1992; Komada et al., 2013). Awaiting better observational estimates using modern techniques, the sediment-exchange and abyssal respiration rate representations in the model perhaps could be improved with a different paradigm at low-oxygen concentration.

Despite these limitations, we can view the rate of O_2 supply by the currents — *e.g.,* in the SMB+SPB, $S_{phys} \approx 10^{-7}$ mmol m^{-3} s^{-1} — as representative of the exchange rate for all dissolved materials being supplied or exported. This is converted into a renewal time scale by dividing it into the ambient concentration within this volume, $O_2 \approx$ 10 mmol m^{-3}, to obtain a renewal time of 10^8 s ≈ 3 years. In the SBB, S_{phys} is larger, albeit more variable, so the renewal time would be smaller.

7 Dispersal and mixing

7.1 Lagrangian trajectories

The most direct measure of pollution dispersal is to integrate passive tracers or Lagrangian particles with a source at the bottom of the deep basins; we choose particle tracking. The Lagrangian trajectory analysis solves (2) for all the released particles that are tracked for a time period T, or else leave the basin at an earlier time (Sec. 2). The relevant metrics for this analysis are $n_{released}(T)$ the number of particles released that are tracked for a minimum time T, and $n_{escape}(t_d)$ the number of particle escaping during a day at tracking time t_d [d] since their release. The instantaneous escape rate at time t_d is given by $n_{escape}(t_d)/n_{released}(T)$ in % per day, and the cumulative fraction of escaped particles at time t by $\Sigma_{t_d}\, n_{escape}(t_d) \,/\, n_{released}(T)$.

For Fig. 17, T is chosen as 57 days as a compromise between wanting many particles and wanting a long tracking period. The result is a total number, $n_{released}(T) = 286,257$, that includes both the summer and winter release sets in the year 2000.

The top panel in Fig. 17 shows that most of the particles escaping vertically across $z =$ - 700 m in the SMB+SPB do so in the basin interiors, *i.e.,* close to their release locations. This is in spite of stronger w values occurring near the basin edges (Fig. 9). The time evolving PDF of particle positions $P[z,t]$ (middle panel) shows that some spread throughout the water column within a month after release, while the majority stay within $\sim$ 200 m of the bottom. The vertical escape rate (Fig. 17, bottom panel) peaks within a week and thereafter slowly declines, while the horizontal escape rate peaks only after a month then also slowly declines. By time T a majority of the particles have escaped vertically, but a bit less than 20% have done so horizontally. Our interpretation of the escape process is that eddy w disperses particles vertically while eddy horizontal currents cause the escapes from the basin boundary with increasing efficacy as the particles ascend toward the pycnocline.

As remarked in Sec. 2, the particle releases are made in 2000, a year without a major sill overflow in the SMB+SPB. From Fig. 13 it is evident that there is low-frequency eddy variability that is under-sampled in our particle releases, and from Fig. 14 that trajectories may be different following sill-overflow events. Thus, although the statistics in

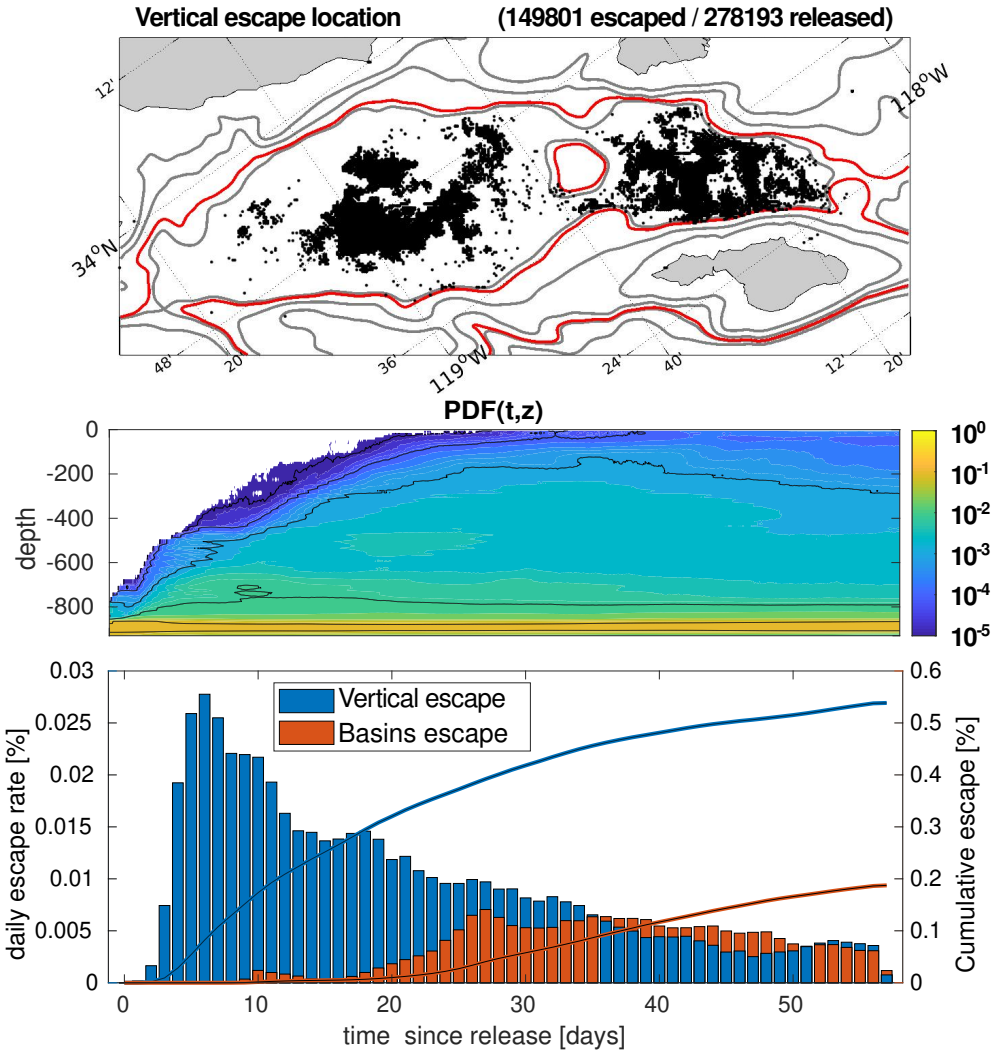

Figure 17. Lagrangian analysis of particle escape patterns during the year 2000 in the SMB+SPB. (Top panel) Horizontals location of the particles that escape vertically from the deep SMB and SPB. (Middle panel) PDF of the vertical distribution of particles in the SMB and SPB as a function of depth and time since release, normalized by the total number at any give time t_d. (Bottom panel) Daily escape fractions shown as bars and cumulative escape ratios shown as lines as a function of time since release, with vertical escape from the deep basin in blue and horizontal escape in red.

Fig. 17 seem reasonably stable, they likely are not fully representative of the range of equilibrium behavior.

7.2 Renewal time estimates

The concept of a water-mass renewal time is somewhat ambiguous, depending on how the water mass volume is defined and how its exchanges with its environment are measured. Here we review several estimates implicit in the evidence presented above.

First consider the mean sill exchange flows in Fig. 7. A renewal time τ is defined by the volume divided by the transport. The basin volumes are 3.7×10^{11} m^3 for water below 700 m depth in the SMB+SPB and 5.9×10^{10} m^3 for water below 450 m depth in the SBB. A rough estimate of the exchange transport across the SMB-SCrB sill is 0.02 m s^{-1} $\times$ 100 m depth $\times$ 3 km width = 6×10^3 m^3 s^{-1}; the transport across the South-SPB sill is much smaller. Thus, $\tau \approx 10^8$ s, or about 2 years. This also is consistent with an assessment of the methane balance (Heintz et al., 2012). The transport across the SBB-Pacific sill is somewhat smaller, but the volume in the SBB is much smaller, so τ is about 1 year (Sec. 7.7.2).

Second, consider the vertical diffusivity estimates by the purposeful tracer release in the SMB (Sec. 1). After the tracers spread to reach the lateral boundaries within about a year since release, the estimated effective vertical diffusvity is $\kappa_v \approx 10^{-4}$ m^2 s^{-1}; hence, a diffusion time $\tau = h^2/\kappa_v$ is about 3 years over a distance $h = 100$ m. This might be an over-estimate if some of the tracers had escaped detection by leaving the deep basins where the measurements were made.

Third, consider the recovery time for O_2 after sill overflow flushing events that inject higher concentrations (Fig. 14). Although individual events vary, the recovery time is around a year in the SBB and somewhat longer in the SMB and SPB.

Fourth, consider the physical supply rate of O_2 as discussed at the end of Sec. 6: about 3 years for the SMB+SPB and about 1 year for the SBB.

Finally, consider the Lagrangian horizontal escape rate for the SMB+SPB (Fig. 17). If we fit an exponential decay function to $F(t) = 1 - n_{escape}(t)/n_{release}(T)$, the final cumulative value of $F(T) = 0.18$ implies an escape time scale of $\tau = T/\ln[F(T)] \approx 3 \times 10^7$ s, or 1 year.

In summary, these independent renewal time estimates are all on the order of a year or more, with the SMB+SPB's probably longer than the SBB's.

8 Summary and discussion

The physical oceanography of the deep basins is still rather poorly known: measurements are few, and the single model simulation reported here has only a few validation standards to assess its abyssal skill.

Nevertheless, the analyses of the present simulation show a number of distinctive features in the Borderland Basins. While they have bounding sill passages and anomalously low bottom oxygen values compared to waters at the same depth outside the basins. The temperature, salinity, and oxygen show continuous vertical profiles across the sill depths, indicating active vertical exchanges. Their seasonal cycles are relatively weak. Their mean currents are strongest on their bounding edge slopes, consistent with eddy-driven topostrophic flow. Eddy and tidal fluctuations are similarly largest at the edges. Part of the eddy variability can be identified with coastal trapped waves, but much of it seems more generally associated with mesoscale eddies in the Southern California Bight. There is considerable low-frequency variability in both currents and water-mass properties, up to and beyond an interannual time scale. Transport pulses occur across the bounding sills driven by cross-sill pressure gradients, sometimes as large overflow flushing events that bring in colder, more oxygenated waters from outside the basins. The 1997-1998 ENSO event caused a large flushing event in all three basins, but more often the overflow events occur independently at the different sills. The deep-basin oxygen balance is comprised of a rather variable physical transport supply rate and more slowly varying respiration and sediment-flux sinks. These rates are much larger in the shallower and more productive SBB than in the SMB+SPB.

A consistent but provisional conclusion emerges about the dispersal of materials within the deep basins. Many aspects of the circulation are relevant to the issue of material dispersal: mean cross-sill transports ventilate the basins; lateral eddy and tidal stirring is efficient at spreading material within the basins; intermittent vertical velocity events raise material up above the height of the confining sills where they are exposed to further lateral eddy dispersal; and rare large sill-overflow flushing events occur. The net effect of these phenomena is a renewal of the deep basin water mass on a time scale on the order of a year or so, although of course we should expect considerable irregularity in particular realizations (*i.e.,* months to years).

An important conclusion of the paper is the limited degree of isolation of the water in the deep borderland basins in spite of their hypoxia and anoxia. As a result, the residence time of water-borne pollutants such as DDT is not very long, although deposition into and release from the sediments may make their presence much more persistent.

Open Research Section

The model code used to generate the simulation is openly available at https://doi.org/10.5281/zenodo.3988618 (Kessouri et al., 2020). The simulations are reproducible using the setup and forcing described in Kessouri, McWilliams, et al. (2021). Due to the large size of the ROMS outputs, only a preprocessed subset, used to generate most of the figures shown in this paper, is provided. It consists of daily averaged currents (u, v, w), tracers (T, S, O_2), and stratification (N^2) interpolated at 450 m and 700 m depth. The simulation data are openly available at https://doi.org/10.5281/zenodo.10689975 (Damien et al., 2024).

Acknowledgments
We thank Dr. Allan Chartrand for inviting us into a study he led on the fate of DDT dumped into the borderland basins during the 1950s-1980s. We also thank our sponsors: National Oceanic and Atmospheric Administration (grant #20160735 03), California Ocean Protection Council (grant #17661), Save Our Coast & Dolphin Watch Foundation, and Tides Foundation. Computational support was provided by the National Science Foundation ACCESS program.

References

Allen, J. S. (1975). Coastal trapped waves in a stratified ocean. *J. Phys. Ocean.*, *5*, 300-325.

Berelson, W. (1991). The flushing of two deep-sea basins, Southern California borderland. *Limnol. Oceanogr.*, *36*, 1150-1166.

Bograd, S., Schwing, F., Castro, C., & Timothy, D. (2002). Bottom water renewal in the Santa Barbara Basin. *J. Geophys. Res. Oceans*, *107*, 3216.

Capó, E., McWilliams, J., Gula, J., Molemaker, M., Damien, P., & Schubert, R. (2024). Abyssal slope currents. *J. Phys. Ocean.*, submitted.

Chartrand, A., Yoshimura, T., Moy, S., & Schinazi, L. (1985). *Ocean dumping under Los Angeles Regional Water Quality Control Board permit: A review of past practices, potential adverse impacts, and recommendations for future action* (Tech. Rep.). California Regional Water Quality Control Board. (47 p.)

Chavez, F. P., & Messié, M. (2009). A comparison of eastern boundary upwelling ecosystems. *Progr. Oceanogr.*, *83*, 80-96.

Collins, L. E., Berelson, W., Hammond, D. E., Knapp, A., Schwartz, R., & Capone, D. (2011). Particle fluxes in San Pedro Basin, California: A four-year record of sedimentation and physical forcing. *Deep-Sea Res. I*, *58*, 898–914.

Craven, D., & Jahnke, R. A. (1992). Microbial utilization and turnover of organic carbon in Santa Monica Basin sediments. *Prog. Oceanog.*, *30*, 313-333.

Damien, P., Bianchi, D., McWilliams, J. C., Kessouri, F., Renault, L., Deutsch, C., & Chen, R. (2022). Enhanced biogeochemical cycling along the U.S. West Coast shelf. *Global Biogeochem. Cycles*, *37*, e2022GB007572.

Damien, P., Kessouri, F., & McWilliams, J. (2024). Southern California Bight ROMS solution [Data set]. *Zenodo*. (doi:10.5281/zenodo.10689975)

Damien, P., McWilliams, J., Bianchi, D., & Kessouri, F. (2023). Modulation of phytoplankton uptake by mesoscale and submesoscale eddies in the California Current System. *Geophys. Res. Lett.*, *50*, e2023GL104853.

Deutsch, C., Frenzel, H., McWilliams, J. C., Renault, L., Kessouri, F., Howard, E., ... Bianchi, D. (2021). Biogeochemical variability in the California Current System. *Progr. Oceanogr.*, *196*, 102565.

Egbert, G., Bennett, A., & Foreman, M. (1994). TOPEX/Poseidon tides estimated using a global inverse model. *J. Geophys. Res.*, *99*, 24,821-24,852.

Emery, K. O. (1954). Source of water in basins off southern California. *J. Mar. Res.*, *13*, 1-21.

Goericke, R., Bograd, S., & Grundl, D. (2015). Denitrification and flushing of the Santa Barbara Basin bottom water. *Deep-Sea Res. II*, *112*, 53-60.

Hamersley, M. R., Turk, K. A., Leinweber, A., Gruber, N., Zehr, J. P., Gunderson, T., & Capone, D. G. (2011). Nitrogen fixation within the water column associated with two hypoxic basins in the Southern California Bight. *Aquatic Microbial Ecology*, *63*, 193–205.

Heintz, M., Mau, S., & Valentine, D. L. (2012). Physical control on methanotrophic potential in waters of the Santa Monica Basin, Southern California. *Limnol. Oceanogr.*, *57*, 420-432.

Hickey, B. (1991). Variability in two deep coastal basins (Santa Monica and San Pedro) off Southern California. *J. Geophys. Res.*, *96*, 16689-16708.

Hickey, B. (1992). Circulation over the Santa Monica-San Pedro Basin and Shelf. *Progr. Oceanogr.*, *30*, 37-115.

Hickey, B. M. (2000). Basin-to-basin water exchange in the Southern California Bight. In D. R. Browne, K. L. Mitchell, & H. W. Chaney (Eds.), *Proceedings of the 5th Channel Islands Symposium* (p. 89-92). Minerals Management Service, Camarillo, CA.

Hughes, M., & Hall, A. (2010). Local and synoptic mechanisms causing Southern California's Santa Ana winds. *Clim. Dyn.*, *34*, 847–857.

Huh, C.-A. (1998). *Historical contamination in the Southern California Bight I: Metals* (Technical memorandum NOS ORC 129). National Oceanic and Atmospheric Administration. (47 p.)

Jackson, G., & et al. (1989). Elemental cycling and fluxes off Southern California. *Eos Trans. AGU*, *70*, 146-155.

Jahnke, R. (1990). Early diagenesis and recycling of biogenic debris at the seafloor, Santa Monica Basin, California. *J. Marine Res.*, *48*, 413-436.

Jørgensen, B. B., Wenzhöfer, F., Egger, M., & Glud, R. N. (2022). Sediment oxygen consumption: Role in the global marine carbon cycle. *Earth-Science Reviews*, *228*, 103987.

Kemnitz, N., Berelson, W. M., Hammond, D. E., Morine, L., Figueroa, M., Lyons, T. W., ... others (2020). Evidence of changes in sedimentation rate and sediment fabric in a low-oxygen setting: Santa Monica Basin, CA. *Biogeosciences*, *17*, 2381–2396.

Kessouri, F., Bianchi, D., Renault, L., McWilliams, J. C., Frenzel, H., & Deutsch, C. (2020). Submesoscale currents modulate the seasonal cycle of nutrients and productivity in the California Current System. *Global Biogeochem. Cycles*, *34*, e2020GB006578.

Kessouri, F., Bianchi, D., Renault, L., McWilliams, J. C., Frenzel, H., Deutsch, C.,

& Molemaker, M. (2020). ROMS-BEC oceanic physical and biogeochemical model code for the Southern California Current System V2020. (https://zenodo.org/records/6886319)

Kessouri, F., McLaughlin, K., Sutulaa, M., Bianchi, D., Ho, M., McWilliams, J., ... Leinweber, A. (2021). Configuration and validation of an oceanic physical and biogeochemical model to investigate coastal eurtrophication in the Southern California Bight. *J. Adv. Modeling Earth Sys.*, *13*, 1-34. (e2020MS002296)

Kessouri, F., McWilliams, J., Bianchi, D., Sutula, M., Renault, L., Deutsch, C., ... Weisberg, S. (2021). Coastal eutrophication drives acidification, oxygen loss and ecosystem change in a major oceanic upwelling system. *Proc. Nat. Acad. Sci.*, *118*, e2018856118.

Kessouri, F., Renault, L., McWilliams, J., Damien, P., & Bianchi, D. (2022). Enhancement of submesoscale eddies by fine scale winds drives high productivity, low oxygen, and low pH conditions in the Santa Barbara Channel. *Geophys. Res. Lett.*, *127*, e2022JC018947.

Komada, T., Burdige, D., Crispo, S., Druffel, E., Griffin, S., Johnson, L., & D.Le. (2013). Dissolved organic carbon dynamics in anaerobic sediments of the Santa Monica Basin. *Geochimica et Cosmochimica Acta*, *110*, 253-273.

Large, W. G., McWilliams, J. C., & Doney, S. C. (1994). Oceanic vertical mixing: A review and a model with a nonlocal boundary layer parameterization. *Rev. Geophys.*, *32*, 363-403.

Ledwell, J., & Hickey, B. (1995). Evidence for enhanced boundary mixing in the Santa Monica Basin. *J. Geophys. Res.*, *100*, 20665-20679.

Ledwell, J., & Watson, A. (1991). The Santa Monica Basin tracer experiment: A study of diapycnal and isopycnal mixing. *J. Geophys. Res.*, *96*, 8695-8718.

Ledwell, J., Watson, A., & Broecker, W. (1986). A deliberate tracer experiment in Santa Monica Basin. *Nature*, *323*, 322-324.

Marchesiello, P., McWilliams, J. C., & Shchepetkin, A. F. (2001). Open boundary conditions for long-term integration of regional oceanic models. *Ocean Modelling*, *3*, 1-20.

McClatchie, S. (2016). *Regional Fisheries Oceanography of the California Current System*. Springer.

Merryfield, W., Cummins, P., & Holloway, G. (2001). Equilibrium statistical mechanics of barotropic flow over finite topography. *J. Phys. Ocean.*, *31*, 1880-1890.

Moore, J. K., Doney, S. C., Kleypas, J. A., Glover, D. M., & Fung, I. Y. (2002). An intermediate complexity marine ecosystem model for the global domain. *Deep-Sea Res. II*, *49*, 403-462.

Mysak, L. (1985). Elliptical topographic waves. *Geophys. Astrophys. Fluid Dyn.*, *31*, 93-135.

Qin, Q., Finnaman, F., Gosselin, K., Liu, N., Treude, T., & Valentine, D. (2022). Seasonality of water column methane oxidation and deoxygenation in a dynamic marine environment. *Geochim. Cosmochim. Acta*, *336*, 219-230.

Renault, L., Masson, S., Arsouze, T., Madec, G., & McWilliams, J. (2019). Recipes for how to force an oceanic model. *J. Adv. Modeling Earth Sys.*, *12*, e2019MS001715.

Renault, L., McWilliams, J. C., Jousse, A., Deutsch, C., Frenzel, H., Kessouri, F., & Chen, R. (2021). The physical structure and behavior of the California Current System. *Progr. Oceanogr.*, *195*, 102564.

Robinson, A. (1964). Continental shelf waves and the response of sea level to weather systems. *J. Geophys. Res.*, *69*, 367-368.

Robinson, D., Pham, A., Yousavich, D., Janssen, F., Wenzhöfer, F., Arrington, E., ... Treude, T. (2024). Iron "ore" nothing: benthic iron fluxes from the oxygen-deficient Santa Barbara Basin enhance phytoplankton productivity in surface waters. *Biogeosciences*, *21*, 773-788.

Schmidt, J., Sin, M., Wu, C., Kittner, H., Arey, J., Hammond, D., & Valentine, D. (2024). Disentangling the history of deep ocean disposal for DDT and other industrial waste off Southern California. *Env. Sci. Tech.*, *58*, 4346-4356.

Schubert, R., Gula, J., Capó, E., Damien, P., Molemaker, M., Vic, C., & McWilliams, J. (2024). The ocean moves downhill near the seafloor and recirculates uphill above. *Nature*. (submitted)

Shchepetkin, A. F., & McWilliams, J. C. (2005). The Regional Oceanic Modeling System (ROMS): A split-explicit, free-surface, topography-following-coordinate oceanic model. *Ocean Modelling*, *9*, 347-404.

Shchepetkin, A. F., & McWilliams, J. C. (2009). Computational kernel algorithms for fine-scale, multi-process, long-term oceanic simulations. In R. Temam & J. Tribia (Eds.), *Handbook of Numerical Analysis: Computational Methods for the Ocean and the Atmosphere* (Vol. 14, p. 121-183). Elsevier.

Sholkovitz, E., & Gieskes, J. (1971). A physical-chemical study of the flushing the Santa Barbara basin. *Limnol. Oceanogr.*, *16*, 479-489.

Skamarock, W. C., & Klemp, J. B. (2008). A time-split nonhydrostatic atmospheric model for weather research and forecasting applications. *J. Comput. Phys.*, *227*, 3465-3485.

Valentine, D. L., Fisher, G. B., Pizarro, O., Kaiser, C. L., Yoerger, D., Breier, J. A., & Tarn, J. (2016). Autonomous marine robotic technology reveals an expansive benthic bacterial community relevant to regional nitrogen biogeochemistry. *Environmental Science & Technology*, *50*, 11057–11065.

Venkatesan, I., amd E. Ruth, G. G., & Chartrand, A. (1996). DDTs and Dumpsite in the Santa Monica Basin, California. *The Science of the Total Environment*, *179*, 61-71.

Venketesan, I. (1998). *Historical Contamination in the Southern California Bight II: Organic Pollutants* (Technical memorandum NOS ORC 129). National Oceanic and Atmospheric Administration. (150 p.)

White, M. E., Rafter, P. A., Stephens, B. M., Wankel, S. D., & Aluwihare, L. I. (2019). Recent increases in water column denitrification in the seasonally suboxic bottom waters of the Santa Barbara Basin. *Geophys. Res. Lett.*, *46*, 6786–6795.

Yousavich, D., Robinson, D., Peng, X., Krause, S., Wenzhöfer, F., Janssen, F., ... Treude, T. (2024). Marine anoxia initiates giant sulfur-oxidizing bacterial mat proliferation and associated changes in benthic nitrogen, sulfur, and iron cycling in the Santa Barbara Basin, California Borderland. *Biogeosciences*, *21*, 789-809.